Resolution of interval velocities from stacking velocity anomalies

John Toldi

Abstract

Stacking velocities contain useful information about laterally variable interval velocities. In recent papers (Rocca and Toldi, 1982, Toldi, 1983), we have discussed how this information can be extracted through a linear theory. In this paper, I discuss the limits on the resolution of interval velocity anomalies as derived from stacking velocities. In other words, exactly how much can one learn about the lateral and vertical extent of a region of anomalous interval velocity from the stacking velocities?

Introduction

In a recent paper, (Toldi, 1983), I made my first attempt at inverting the stacking velocities from a field dataset. The dataset was unusual in that the only reflectors in the entire dataset were very closely spaced in depth. As a consequence the results were rather unsatisfactory. In particular, the vertical resolution was very poor.

This brought up the question of how much vertical resolution of interval velocity anomalies is actually possible from the stacking velocities from one reflector. A related question is whether stacking velocities can resolve the interval velocities to within a vertical spacing less than that between reflectors. Note that the Dix formula provides one velocity between each pair of reflectors. Thus, the velocities derived through this linear stacking velocity method will have at worst a vertical resolution equal to that provided by the Dix formula.

Because the method is linear, many tools are available for studying resolution. In this paper, I concentrate on what can be learned from the singular value decomposition of the matrix that relates anomalous interval velocities to stacking velocities.

The linear theory

For a given reflector at depth z_r, the linear theory provides the stacking slowness response as a function of midpoint y, to an impulse of anomalous interval slowness at position (y_{an},z_{an}). More precisely,

$$\Delta w_s(y,z_r) = G(y,z_r,z_{an},y_{an})\,\Delta w_{in}(y_{an},z_{an})\,\Delta y_{an}\,\Delta z_{an} \tag{1}$$

where Δw_s , Δw_{in} and G are the anomalous stacking slowness, the anomalous interval slowness, and the impulse response respectively. The geometry is shown in figure 1.

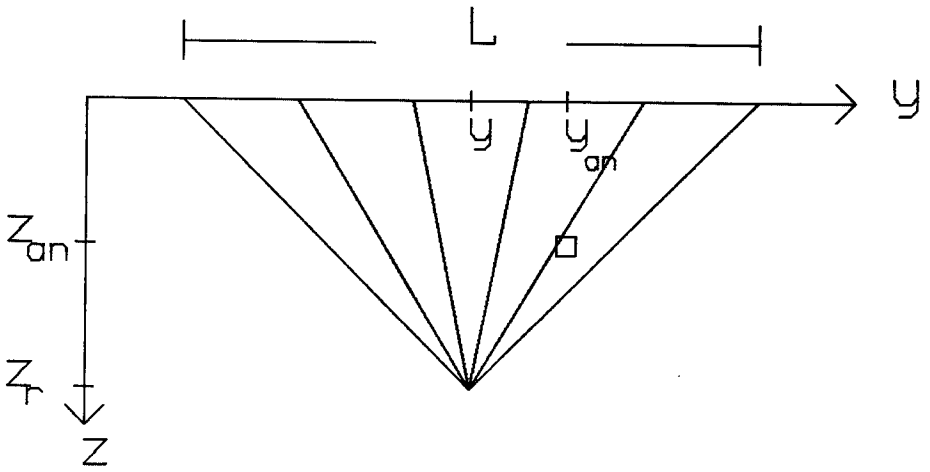

FIG. 1. Geometry for constant background velocity. Shown are a few raypaths to the reflector at depth z_r for the midpoint gather at y. The maximum offset is L. The impulse of anomalous interval slowness has coordinates (y_{an},z_{an}).

For completeness I include the impulse response, G,

$$G(y,z_r,z_{an},y_{an}) = \frac{15z_r}{L^2L'}\left[3\left[\frac{2y}{L'}\right]^2 - 1\right]\left[1 + \frac{L^2}{4z^2}\left[\frac{2y}{L'}\right]^2\right] \tag{2}$$

In equation 2,

$$L' = effective\ cable\ length = \frac{(z-z_{an})}{z}L$$

As can be seen from figure 2, the stacking slowness at one midpoint will be influenced by interval slowness anomalies within half an effective cable length to either side. The

effective cable length L' is thus the aperture of the filter that relates interval slowness to stacking slowness.

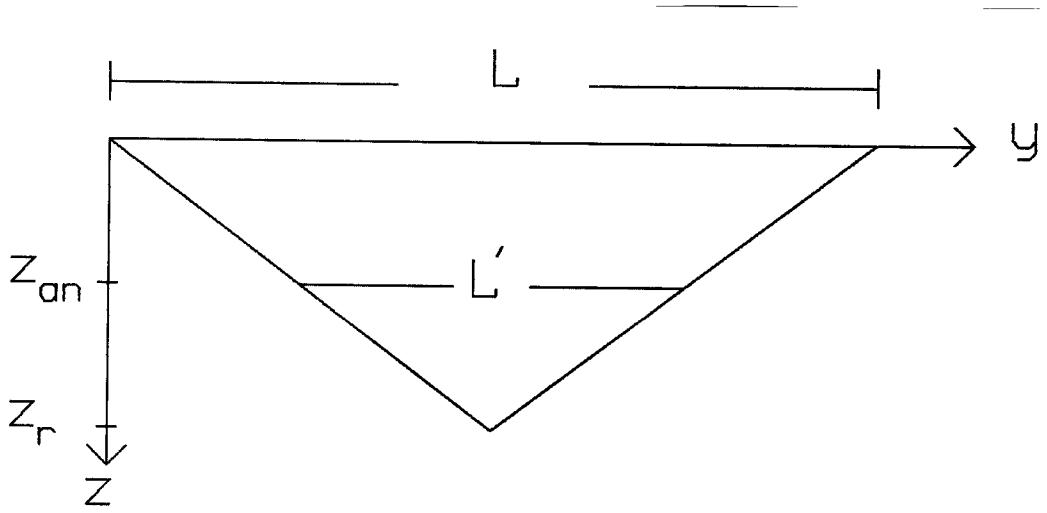

FIG. 2. L is the maximum offset, i.e. the cable length. L' is the effective cable length for reflector at depth z_r and anomaly at depth z_{an}.

Superposing the effects of impulses at all depths and midpoints, one finds:

$$\Delta w_s(z_r,y) = \int\int G(z_r,y,y_{an},z_{an})\, \Delta w_{in}(y_{an},z_{an})\, dy_{an}\, dz_{an} \tag{3}$$

By expressing the interval velocity distribution in terms of a set of basis functions one can convert the integral of equation 3 into a sum. In later portions of this paper, I will discuss a specific choice of basis functions. For the present I assume a general set of n orthonormal basis functions $h_j(y_{an},z_{an})$, such that:

$$\Delta w_{in}(y_{an},z_{an}) = \sum_{j=0}^{n} m_j h_j(y_{an},z_{an}) \tag{4}$$

The m_j are the expansion coefficients.

Inserting equation 4 into 3 yields:

$$[\Delta w_s]_i = \sum_{j=0}^{n} G_{ij} m_j \tag{5}$$

where,

$$G_{ij} = \int\int G(z_r, y, y_{an}, z_{an})\, h_j(y_{an}, z_{an})\, dz_{an}\, dy_{an} \qquad (6)$$

The subscript i refers to the point in the data space: each $[\Delta w_s]_i$ is the anomalous stacking slowness for a specific reflector at a specific midpoint. Treating the data as one big vector makes for the simple notation of equation 5.

Basis functions-Model parameterization

In a paper in the last SEP report (Toldi, 1983), I discussed the need for a space domain implementation of the linearized stacking velocity method. This need arose from a desire to use stacking velocities from reflectors that were not continuous across the entire section of interest. Furthermore, in a space domain method, weights can be attached to the stacking velocity picks according to their reliability. These weights can vary along a reflector.

In order to implement the linear theory, one must express the interval velocity model in terms of some set of basis functions. (see equations 3,4 and 5) The solution will naturally be restricted to the space spanned by the basis functions. Thus, in choosing a set of basis functions, one is already making decisions as to the possible resolution of the model.

In this paper I use basis functions that are sines and cosines in the midpoint direction, and thin strips in depth. Figure 3 shows one such basis function. In earlier work with this theory I used these same basis functions when I Fourier transformed the whole system over midpoint and then looked at thin strips for each Fourier component. The difference is that now I will look at the entire system at once.

The reason for retaining the lateral Fourier components as basis functions in the analysis is that in our earlier work we gained considerable insight from the transfer function (the lateral Fourier transform of the impulse response G). Specifically, the response of the operator is a function of the relationship of the wavelength of anomaly to the effective cable length. Using strips in depth allows the boundaries between basis functions to fall along layer boundaries. This is desirable when I consider depth resolution. Furthermore, the strips also form an orthogonal set, which simplifies the computations.

In using laterally sinusoidal basis functions one must decide on a highest spatial frequency to use. In this study, I use the width of a Fresnel zone as my guideline. Specifically, I make the maximum lateral wavelength be equal to the width of a Fresnel zone at the bottom of the model. More properly, this maximum should be a function of depth. That is, allow very short wavelengths up in the shallow portion then gradually bring down the maximum as depth increases.

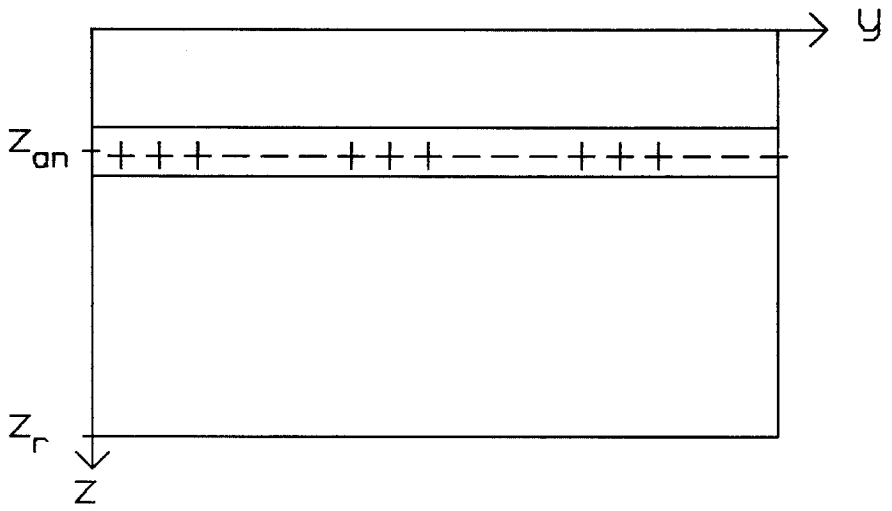

FIG. 3. Basis function at depth z_{an} and thickness Δz_{an}. In the lateral direction it is a sine with period equal to 1/3 the width of the model.

In the first part of this paper I consider what can be learned about the overlying laterally variable velocities from the stacking velocities determined from one reflector. The model is thus the following:

depth of reflector = 5000 ft.
width of model = 25600 ft.
cable length = 4800 ft
maximum k_y = 24 --> shortest wavelength = 1066 ft.
number of anomalous depths = 10, each 500 ft thick.
stacking slownesses recorded at 64 midpoints

Thus a vector in the data space has 64 elements. A model space vector has (2x24-1)x10 =470 elements, one for each basis function. The factor of 2 enters because for each frequency of basis function there is a sine and a cosine. Thus the dimensions of the matrix G are 64 by 470.

Model space eigenvectors

The resolution of a particular component of the interval velocity model is related to how strongly that component affects the data. Components which have little or no effect on the data will be poorly resolved, whereas those which most affect the data will be best

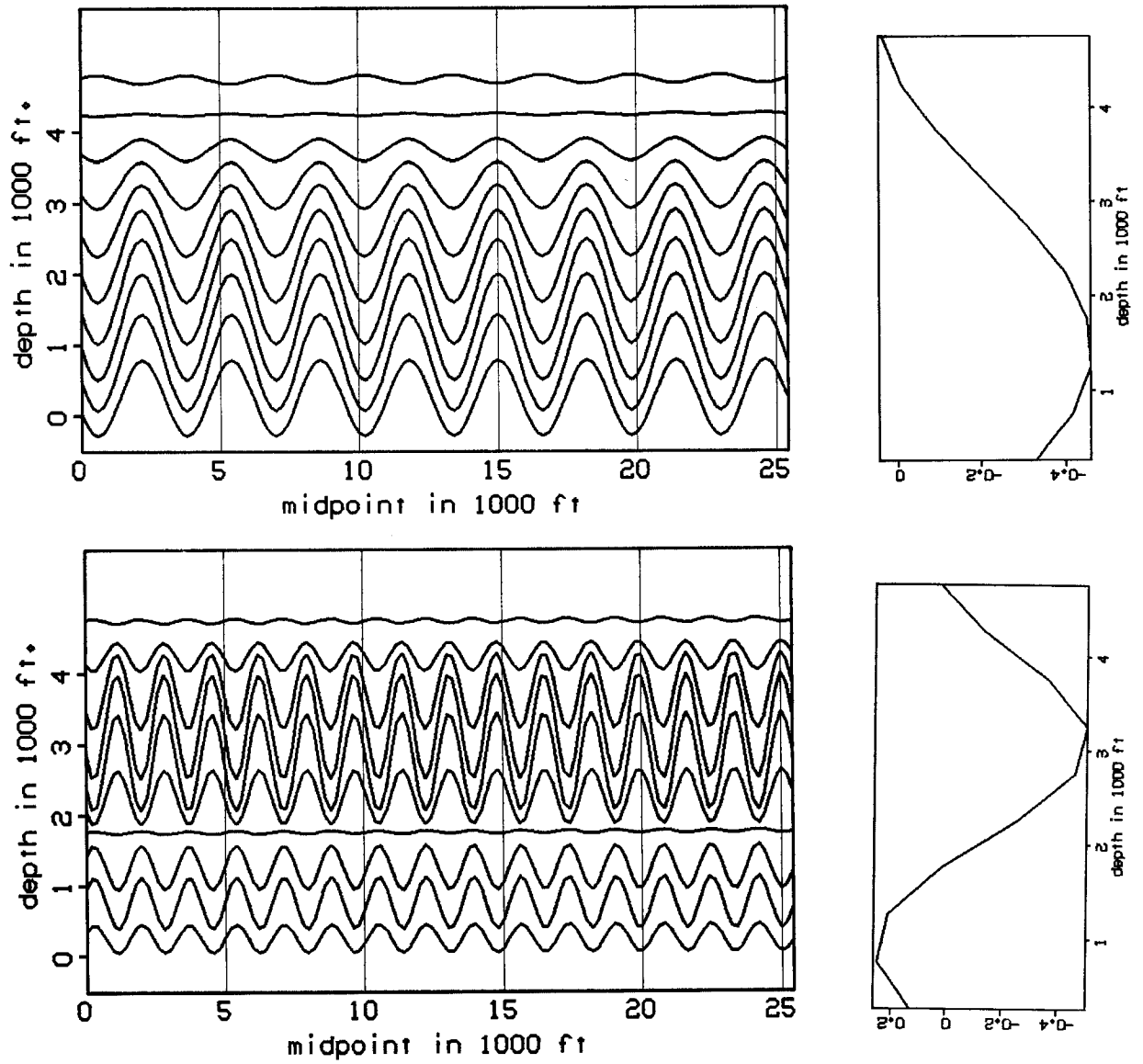

FIG. 4. Model space eigenvectors. Each one is a sinusoid laterally, with the vertical distribution of amplitude shown at right.

resolved. The singular value decomposition (SVD) of G (see Strang, 1980, Aki and Richards, 1980) is particularly useful in the study of resolution, because it allows one to directly examine how well each component of the model can be determined.

The singular value decomposition of the matrix **G** leads to:

$$\mathbf{G} = \mathbf{U}\Lambda\mathbf{V} \tag{7}$$

where **U** is the matrix of data space eigenvectors, **V** the matrix of model space eigenvectors, and Λ a matrix with entries (the eigenvalues) along the diagonal. Note that these

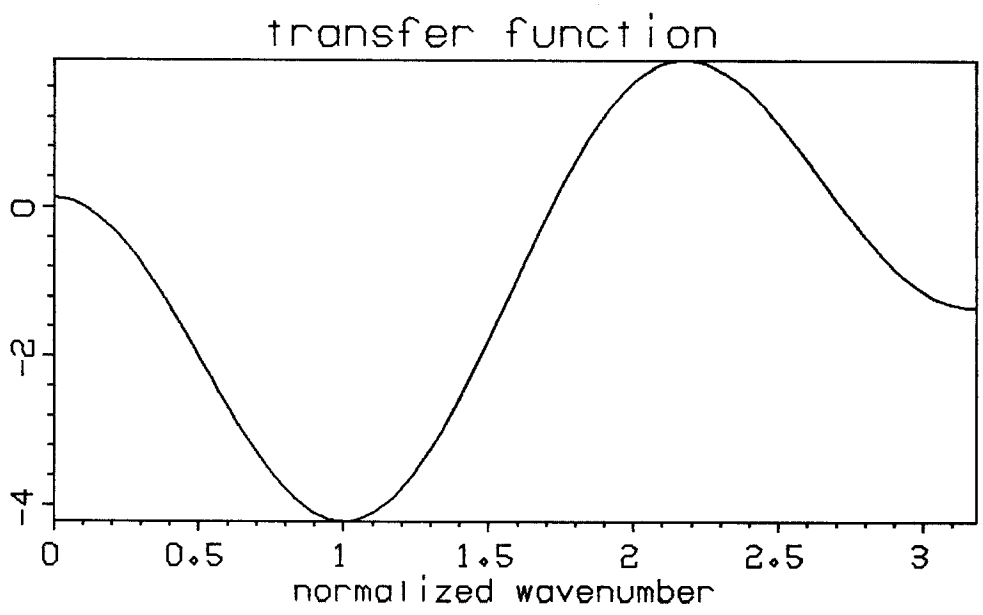

FIG. 5. Transfer function. The horizontal coordinate has been normalized in such a way that the scale now refers to the number of wavelengths per effective cable length.

eigenvalues are actually the eigenvalues of the matrix $\mathbf{G}^t\mathbf{G}$. Shown in figure 4 are two of the model space eigenvectors. Not surprisingly, they are lateral sinusoids with amplitude modulated in depth. At the right of figure 4 is a vertical slice through each eigenvector. The vertical slices emphasizes the amplitude as a function of depth.

The amplitude distribution shown in the vertical slices can be best understood with the help of the transfer function shown in figure 5. The horizontal scale is the midpoint wavenumber axis, normalized in such a way that the units are wavelengths of anomaly per effective cable length. For example, the response at k = 1, is the stacking slowness response to an interval slowness anomaly with wavelength equal to the effective cable length.

Suppose that the wavelength of the anomaly in the earth is fixed at a particular value, say 1 cable length. Thus, the response to an anomaly at the surface of wavelength one cable length will be -4 (i.e. the response at k = 1). Then as the depth of the anomaly increases, the effective cable length will decrease. The corresponding response can be found by moving back along the k axis (towards the origin) an appropriate amount. As the depth of anomaly approaches the depth of the reflector, the response will approach the

response at $k = 0$. This is due to the fact that when the effective cable length gets very small, every frequency starts to look like the zero frequency.

Now return to the vertical slices of figure 4. Each of these curves is just the appropriate portion of the transfer function: each one starts at the surface with a response determined by the number of wavelengths per actual cable length, then moves back towards the response at zero frequency.

Eigenvalues

Now I would like to turn my attention to the eigenvalues. The magnitude of the eigenvalue associated with each of the eigenvectors described in the last section is a measure of how strongly that component affects the data. Because the smaller dimension of the matrix **G** in equation 7 is 64, one would expect at most 64 non-zero eigenvalues.

Figure 6 shows the eigenvalues, plotted in order of decreasing size. Because the sine and the cosine of each wavelength are equally well determined, the eigenvalues come in pairs. Note that there are only 47 non-zero values, corresponding to the 47 sines and cosines. This limitation occurs because the data space can only contain components that are linear combinations of the sines and cosines. Note also that the non-zero eigenvalues range from 1 to 13.

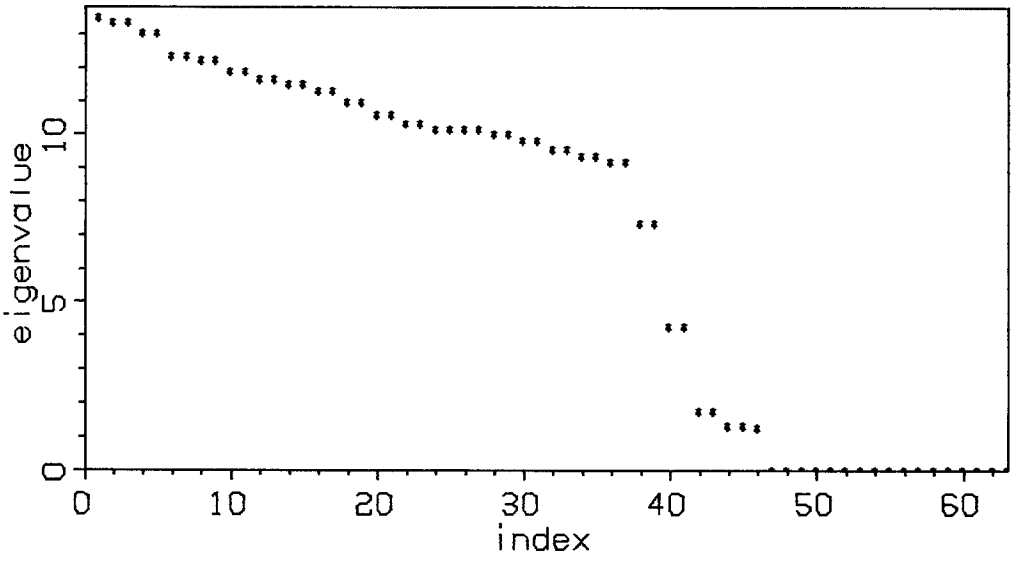

FIG. 6. Eigenvalues in order of decreasing size.

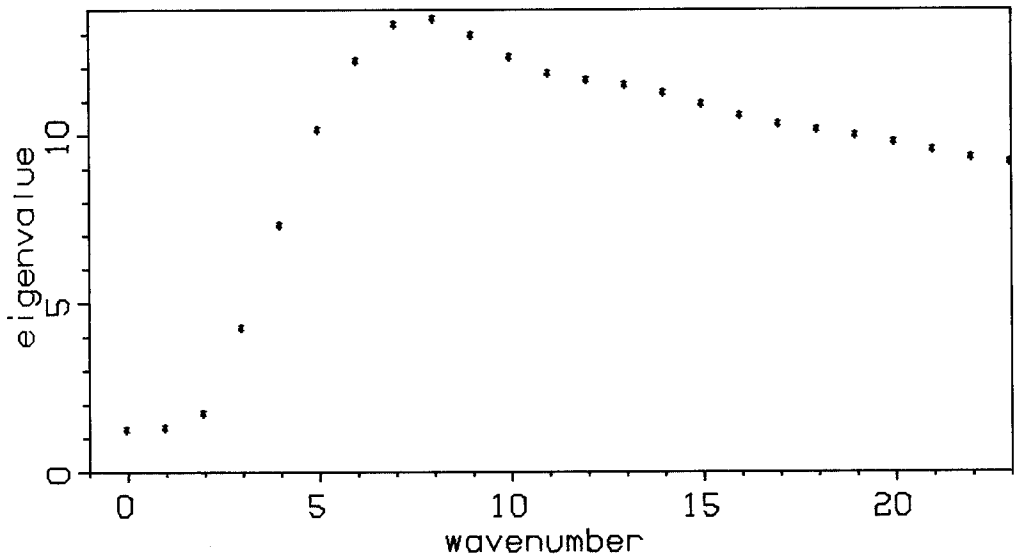

FIG. 7. Eigenvalue versus wavenumber of eigenvector. Note that the low wavenumber (i.e. long wavelength) components are the most poorly determined.

An even more revealing way to look at the eigenvalues is to plot eigenvalue versus wavenumber of the corresponding eigenvector. Figure 7 makes this comparison. It shows that the response is fairly flat for the higher wavenumbers, but drops off sharply for the low wavenumbers.

In particular, the three lowest wavenumbers all have eigenvalue of about 1 - a factor of 10 less than most of the others. The eigenvector with the lowest eigenvalue, is the DC, or zero frequency component. The next two have wavelengths equal to the width of the entire model and half the model respectively. The width of the model is about 6 cable lengths. Thus all three of these poorly determined components have wavelengths of 3 cable lengths or more.

This result was to be expected from the earlier discussion of the transfer function. Not only is there a zero in the response at a normalized wavenumber of .1, but the entire response from about .2 back to the origin is weak (see figure 5). Thus all wavelengths of about 5 effective cable lengths or greater are weakly determined. The component with wavelength equal to 3 cable lengths has, over most of its depth range, an effective cable length of 5 or greater, and is therefore weakly determined.

A physical reason for this is that the linear filter that we are examining here is like a second derivative operator with a small DC component added in. The space domain impulse response (equation 2) is plotted in figure 8. The long wavelength anomalies appear to be approximately constant within the aperture, and are thereby nearly eliminated by the

operator. In an earlier paper, we pointed out that the response is non-zero for the zero frequency component; the lesson here is that although it is non-zero, it is very weak.

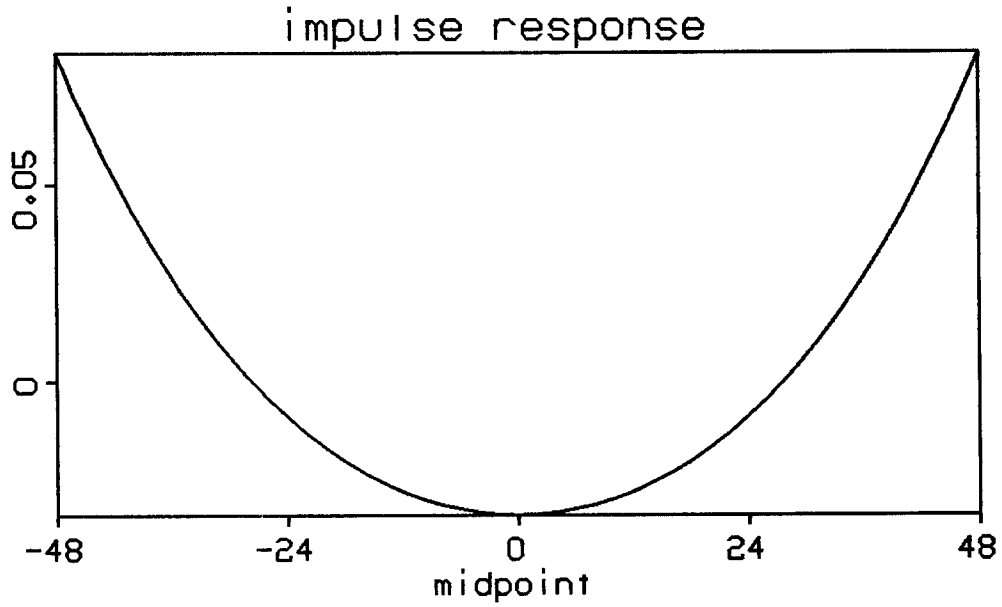

FIG. 8. Space domain impulse response of the filter. Appearance is that of a second derivative operator.

The problems with determining the low frequencies should, however, not cause too much concern. After all, this is a perturbation method: in applying it one is looking for the anomalous interval velocity distribution, based on some underlying background distribution. These long wavelength velocity variations belong most naturally in the background distribution.

Incorporating lateral variations into the background distribution may at first seem troublesome, because the entire development assumed a constant, or at most depth-variable background velocity. But notice that the velocity does not enter at all into the impulse response of equation 2. Thus the background velocity could just as well be required to be laterally constant over an effective cable length.

A glance at the transfer function of figure 5 shows that there are zeroes at regular intervals, not only near the origin. Why don't these also provide problems? Because the slope of the curve is fairly steep at the later zero-crossings, a zero will appear only at certain isolated combinations of frequency, depth of anomaly and depth of reflector. Furthermore, because the zero will show up at certain combinations of wavelength and effective cable length, it will show up at different wavelengths for different depths. This is quite

unlike the long wavelength case, where the same weak response is seen at all depths.

Depth resolution

In the final part of this paper I would like to turn to the question of depth resolution. A useful indicator of resolution is the projection matrix $\mathbf{V}_p\mathbf{V}_p^t$, where $\mathbf{V}_p$ is the matrix of model space eigenvectors that have non-zero eigenvalues, i.e. the principal part of the model space. If there were no model null space, $\mathbf{V}_p\mathbf{V}_p^t$ would be a diagonal matrix. Instead, it has some spread about the diagonal.

Because of the non-local nature of my basis functions, looking at a row of $\mathbf{V}_p\mathbf{V}_p^t$ does not provide the resolution information that I seek. It would provide a measure of resolution in Fourier space. I would rather look specifically in the space domain. Thus, in the examples that follow, I look at the effect of $\mathbf{V}_p\mathbf{V}_p^t$ upon a space domain impulse in my model.

Recall that the model consists of a series of 10 thin strips of thickness 500 feet. The reflector is at a depth of 5000 feet, and the cable length is 4800 feet. Although the full width of the model is 25000 feet, the figures that follow will show only the central portion.

Each curve of figure 9a shows the interval velocity distribution in horizontal strip. Thus, Figure 9a shows an impulse of anomalous interval velocity in the first depth strip (i.e. at depth 250 feet) at midpoint 13. Note that it is not a true impulse, but rather the closest thing to an impulse possible within the space spanned by the basis functions.

Figure 9b shows the results for the same spike, only now projected onto $\mathbf{V}_p$ space. Clearly the spike has been smeared in depth, although notice that the result does have its maximum amplitude at the surface and decays with depth. The main central peak seems to have decayed by a depth of about 2000 feet. The projection onto $\mathbf{V}_p$ space has caused certain wavelengths to be strongly enhanced, and others entirely eliminated. Thus the sidelobes are quite noticeable.

Figure 10 shows the results for an impulse at the same midpoint coordinate, but now at a depth of 2250 feet. The impulse has clearly been smeared over at least five depth strips (2500 feet). The important feature is that it is still recognizable as having been at a depth of approximately 3000 feet. Thus, although the resolution is imperfect, some depth resolution within the layer is possible. In particular, we could clearly discriminate between the cases shown in figures 9 and 10.

Figure 11 shows the results for an impulse directly above the reflector. The original location of the impulse is not even recognizable. For an anomaly on top of the reflector, the effective cable length is nearly zero. Thus all components of the anomaly have the weak

a

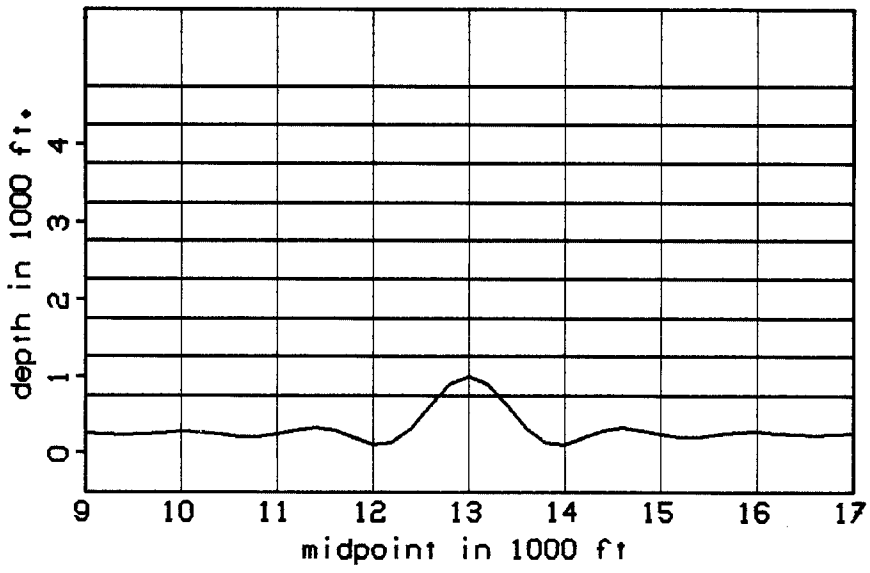

b

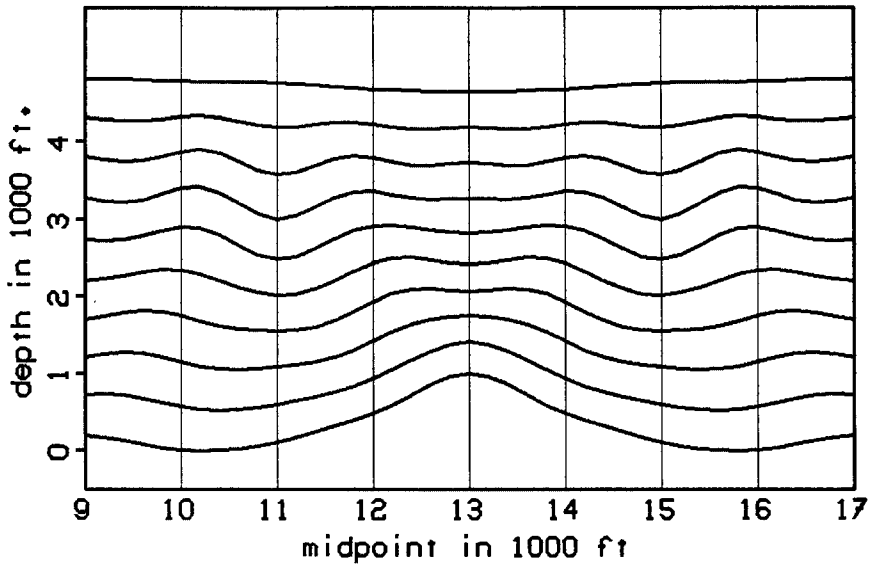

FIG. 9. a) Impulse at midpoint=13000 ft. and depth=250 ft. Only the central portion of the model is shown. b) Impulse projected onto V_p space.

low frequency response.

Offset ranges

In a paper in the last report, I discussed the possible benefits of using stacking velocities determined over independent ranges of offsets. This was based on the suggestion by Shuki Ronen, that taking a couple of ranges might greatly improve the vertical resolution. The basic idea is that the zeroes of the transfer functions fall at different frequencies for

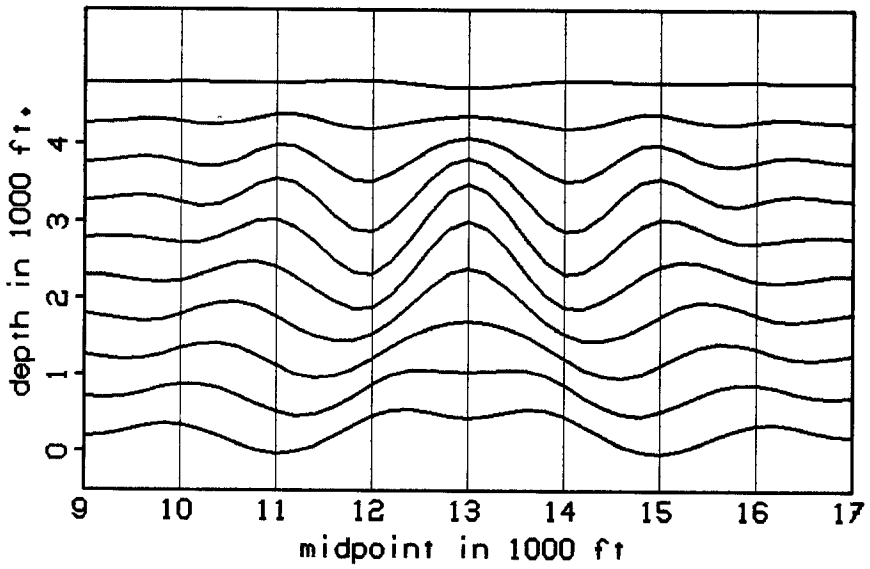

FIG. 10. Impulse at 2250 feet projected onto V_p space.

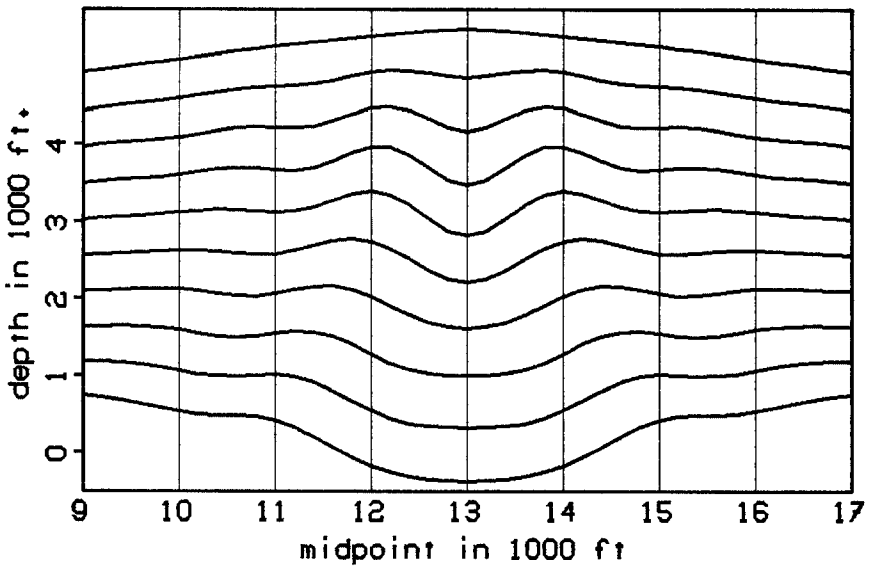

FIG. 11. Impulse directly above reflector (i.e. at 4750 feet) projected onto V_p space.

different offset ranges. Thus the model space has a much smaller null space.

The methods of this paper are ideal for testing the offset range idea. Using a model similar to the one that I have used so far, I derived the matrix **G**, for the case of two offset ranges (0-3200 feet and 3200-4800 feet). For ease of computation, I decreased the number of depth strips from 10 to 5, thereby increasing their thickness from 500 feet to

1000 feet. To make a fair comparison, I also reran the full offset range example with this new model.

Figures 12a through 12e show the results of projecting onto V_p space for the single and double offset ranges. Shown are the results for impulses at depths of 500, 1500, 2500, 3500 and 4500 feet. The resolution offered by the offset ranges is strikingly better for the shallow impulses (figures 12a through 12c). For the deeper impulses, (figures 12d and 12e), the results are more similar, probably because of the short effective cable lengths involved at those depths.

Conclusions

In this paper I have examined the limits on the vertical and horizontal resolution of interval velocities as derived from stacking velocities. This study has shown that useful information about the depth of interval velocity anomalies is available from stacking velocities. This was even true in the extreme case of the single reflector.

Problems do arise with long-wavelength lateral variations in interval velocity. These long wavelengths would best be incorporated into the assumed background distribution. Only when the noise level is very low should they be allowed to enter into the calculations.

Finally, a method that determines stacking velocities over independent ranges of offsets seems particularly interesting. With only two offset ranges the method provided considerably better vertical and lateral resolution than did the standard full offset method.

REFERENCES

Aki, K., and Richards, P., Quantitative seismology: San Francisco, W.H Freeman, 1980.
Rocca, F. and Toldi, J., 1982, Lateral velocity anomalies: SEP-32, p.1-13.
Strang, G., Linear Algebra and its applications: Academic Press, 1980
Toldi, J., 1983, Lateral velocity anomalies - model study: SEP-35, p.3-17.
Toldi, J., 1983, The linear stacking slowness method for a field dataset: SEP-37, p.17-26.

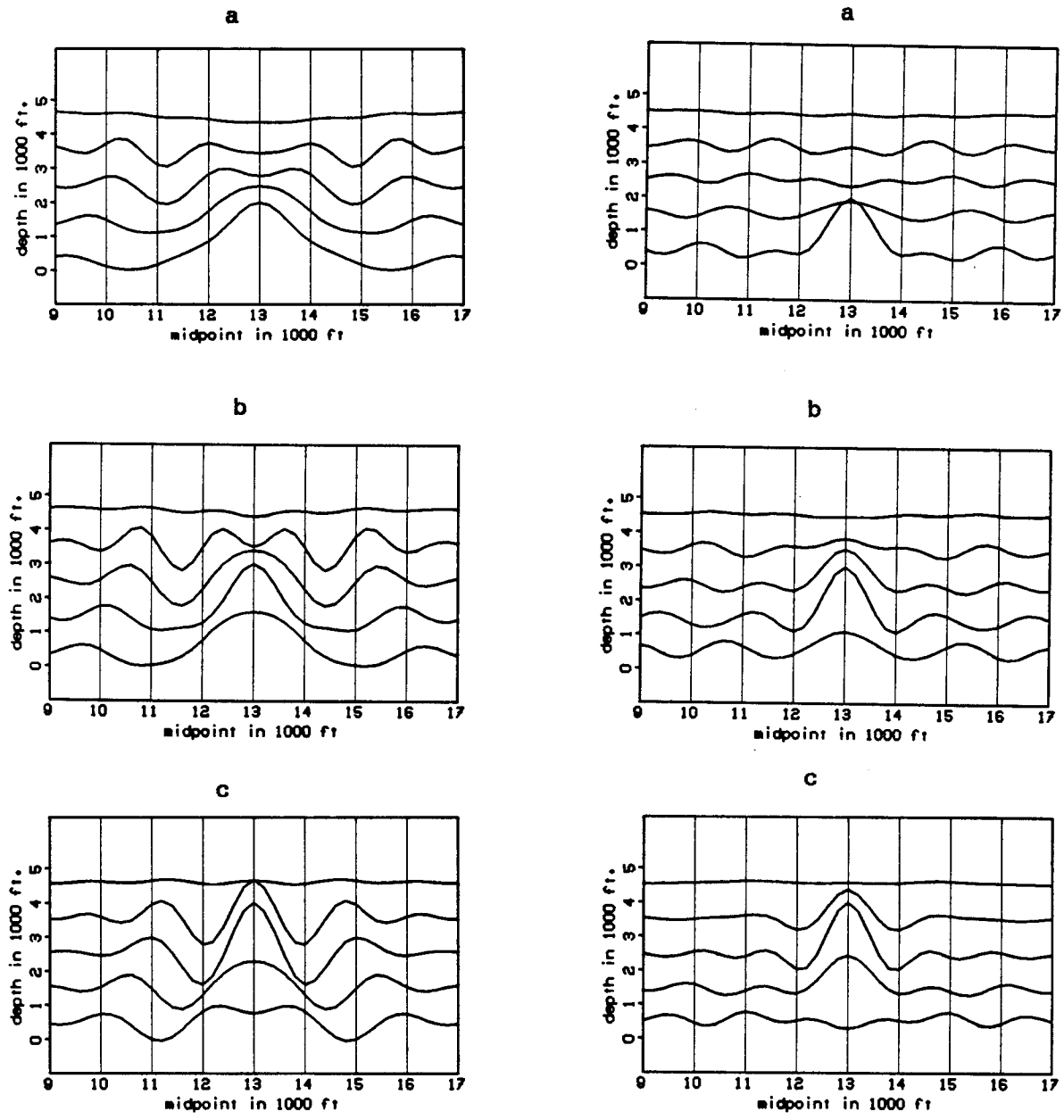

FIG. 12. Full offset range, left, versus two independent offset ranges, right. The impulses are at depths, a) 500 feet, b) 1500 feet, c) 2500 feet

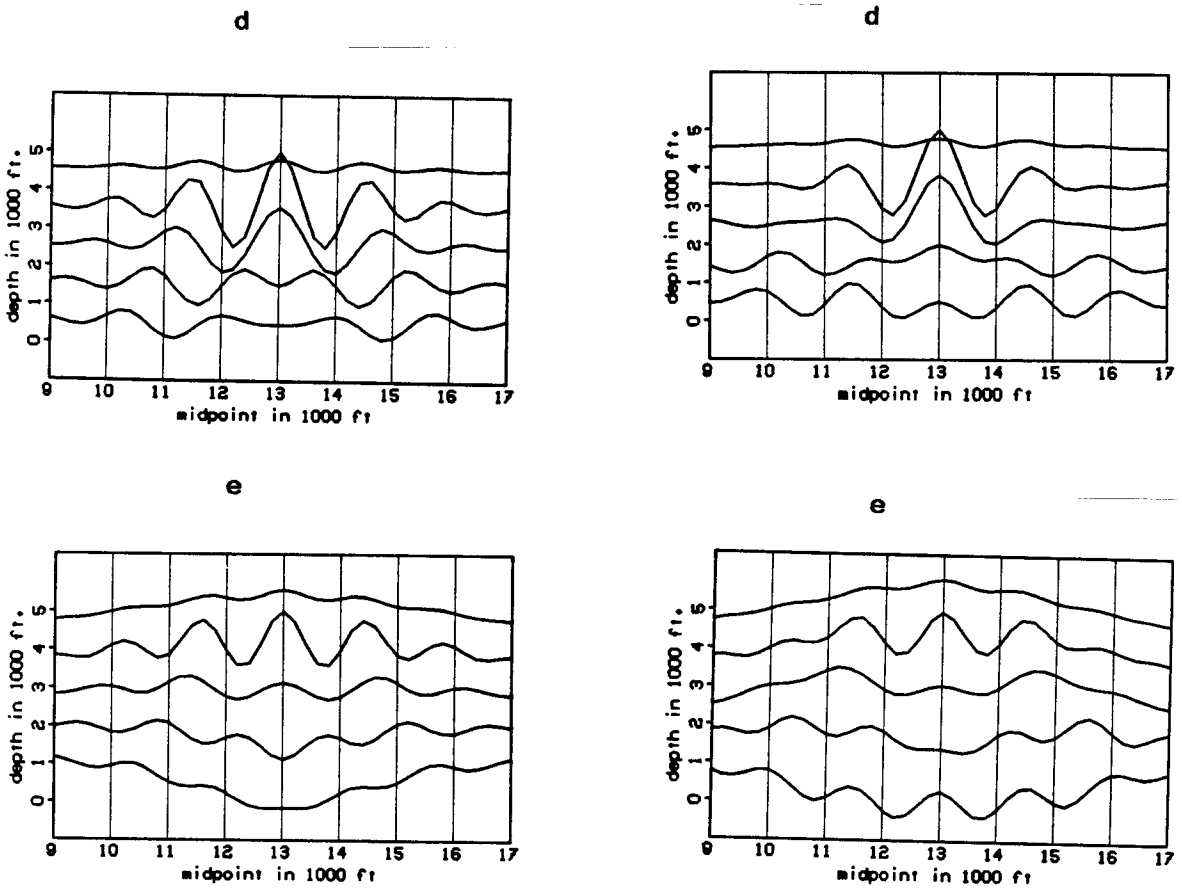

FIG. 12. Full offset range, left, versus two independent offset ranges, right. The impulses are at depths, d) 3500 feet, b) 4500 feet